Catalytic Combustion of n*-Hexane Over Alumina Supported Mn–Cu–Ce Catalysts*

Maria Roxana Morales, Fabiola N. Agüero & Luis E. Cadus

Catalysis Letters

ISSN 1011-372X

Catal Lett
DOI 10.1007/s10562-013-1083-6

Springer

Catal Lett
DOI 10.1007/s10562-013-1083-6

Catalytic Combustion of *n*-Hexane Over Alumina Supported Mn–Cu–Ce Catalysts

Maria Roxana Morales · Fabiola N. Agüero · Luis E. Cadus

Received: 9 January 2013 / Accepted: 30 July 2013

Abstract Supported MnCuCe and MnCe mixed oxides catalysts were prepared and evaluated in *n*-hexane combustion reaction. They presented an excellent catalytic activity in total combustion of *n*-hexane. Catalysts were characterized by means of XRD, XPS, SBET and TPR techniques. The addition of Cu did not enhance the catalytic activity of MnO_x/Al_2O_3 due to the formation of the complete Mn_2CuO_4 spinel. The presence of cerium favored the formation of manganese oxide species with low crystallinity, with high oxygen mobility and high oxygen vacancies. A higher content of Ce was necessary to obtain catalysts with higher oxidation state of Mn and Ce species.

Keywords Manganese · Copper · Cerium · Catalytic oxidation · Alumina

1 Introduction

Catalytic oxidation is one of the most developed techniques used for the elimination of VOCs, which are considered as major air pollutants [1–5]. Two groups of catalytic materials are usually employed for total oxidation of VOCs in air streams, supported or unsupported noble metal catalysts (mainly Pt and Pd), and transition metal oxide-based catalysts. Although, the former usually have higher activities toward oxidation reactions [6, 7], the high costs, their sensitivity to poisoning by chlorine and the formation of toxic polychlorinated compounds when used for total oxidation of chlorinated VOCs [8, 9] limit their wide applications. Therefore, transition metal oxides and their binary mixtures [10–12] have been widely evaluated for the total oxidation of VOCs. $CuO–CeO_2$ and CuO/CeO_2 catalysts were very effective in the preferential oxidation of CO [13–15] at low temperatures, to an extent comparable to supported platinum catalysts. Their high activity was attributed to the high oxygen storage capacity of ceria [16, 17], the facile Ce^{4+}/Ce^{3+} redox cycle [18], and the synergistic effect between CuO and CeO_2 [19]. Better redox properties than those of CeO_2 can be obtained by incorporating metal ions such as Zr^{4+} [20], Sn^{4+} [21] or Mn^{x+} [22] into CeO_2 to form the solid solution $Ce_{1-x}M_xO_2$. Manganese oxides, which have a high oxygen storage capacity, have exhibited high activity in catalytic reactions [23, 24]. Hopcalite, a mixed oxide mixture that is based on copper and manganese oxides, has been used for many years to remove toxic gases. Tang et al. [25] demonstrated that $MnO_x–CeO_2$ mixed oxides were highly active in the oxidation of formaldehyde at low temperature and exhibited a much higher activity than pure ceria or MnO_x alone. Li et al. [26] also showed that the addition of manganese into CeO_2 to form $Ce_{1-x}Mn_xO_2$ solution increased the mobility of lattice oxygen and considerably improved its performance and the corresponding to $CuO/Ce_{1-x}Mn_xO_2$ catalyst in the complete oxidation of benzene. In a previous work, it was shown that MnCu catalyst with 9:1 molar ratio prepared by the co-precipitation method presented an excellent catalytic performance in VOCs combustion reaction and a very good stability. It was demonstrated that a little amount of copper improved the catalytic performance and favoured a poor crystalline manganese oxide which contains the $Cu_{1.5}Mn_{1.5}O_4$ incomplete spinel phase [27]. In last years, the use of structured supports has being required in order to avoid high pressure drops. These

M. R. Morales · F. N. Agüero (✉) · L. E. Cadus
Instituto de Investigaciones En Tecnología Química (INTEQUI), UNSL-CONICET, Casilla de Correo 290, 5700 San Luis, Argentina
e-mail: fnaguero@unsl.edu.ar

Published online: 15 August 2013

structures as monoliths usually made of ceramic or metallic materials are generally covered with an alumina layer that acts as the support of the active phase [28]. Thus, in the present work, we investigate the addition of Cu and Ce to an alumina supported manganese oxide in an attempt to develop more efficient catalyst formulations. The catalytic performance of these materials in *n*-hexane combustion was compared to that of the corresponding supported single oxide catalyst in order to investigate the correlation between physicochemical characteristics and reactivity of optimized materials.

2 Experimental

2.1 Catalysts Preparation

The catalysts were prepared by impregnation to incipient wetness of the Al_2O_3 supports previously dried under vacuum at 137 °C for 3 h, with aqueous solutions of $Mn(CH_3COO)_2{\cdot}2H_2O$ (Fluka), $Cu(CH_3COO)_2{\cdot}H_2O$ and $Ce(CH_3COO)_3{\cdot}6H_2O$. The impregnation was carried out in multiple stages with drying in between at 80 °C for 2 h. The amount of added solution was the necessary to obtain a manganese loading equivalent to three theoretical monolayers of Mn_2O_3. Finally, the samples were dried at 100 °C overnight and calcined at 500 °C for 3 h. The obtained catalysts were called $(Mn_{1-x}Cu_x)_{1-y}Ce_y$–Al_2O_3 with $x = 0$ and 0,1; $y = 0$, 0.1, 0.2 and 0.3.

2.2 Catalysts Characterisation

2.2.1 BET Specific Surface Area Measurements (SBET)

The specific surface area of the samples was calculated by the BET method from the nitrogen adsorption isotherms obtained at 77 K. A Gemini V from Micromeritics apparatus was used.

2.2.2 X-ray Diffraction (XRD)

XRD patterns were obtained by using a Rigaku diffractometer operated at 30 kV and 25 mA by employing Cu Kα radiation with Nickel filter ($\lambda = 0.15418$ nm).

2.2.3 Temperature Programmed Reduction (TPR)

The TPR was performed in a quartz tubular reactor using a TCD as detector. Samples of 100 mg were used. The reducing gas was a mixture of 5 vol % H_2/N_2, at a total flow rate of 30 ml min^{-1}. The temperature was increased at a rate of 5 °C min^{-1} from room temperature to 700 °C. The deconvolution procedure included the following steps: (i) selecting the minimum number of peaks which could describe each profile; (ii) fitting the profiles by imposing the same full width at half maximum (FWHM) for all component peaks; (iii) optimising the deconvolution by allowing small deviations in the FWHM.

2.2.4 X-ray Photoelectron Spectroscopy (XPS)

XPS data were obtained with a Multitecnic UniSpecs equipment with a dual X ray source of Mg/Al and an hemispheric analyzer PHOIBOS 150. A pass energy of 30 eV and an Al anode operated at 100 W was used. The pressure was kept under 2×10^{-8} mbar. The charge effect was corrected using as reference the Al2p peak (74.5 eV).

2.3 Catalytic Evaluation

A glass reactor of fixed bed at atmospheric pressure was used. Data were obtained in steady state. A sample of 200 mg (0.15–0.18 mm particle diameter) diluted with 2,272 g of glass particles of the same size. The reacting stream was 300 ml/min^{-1} with a composition of 4,788 ppm of hexane diluted in synthetic air. The space velocity used in the catalytic test was 1,894 h^{-1}. The gaseous mixtures were analyzed before and after reaction by gas chromatography using a Buck Scientific Mod 910 equipped with a FID detector, a methanizer and a Carbowax 20 M/ChromosorbW column. The kinetic experiments were conducted at constant temperatures (140, 150 and 160 °C) and the reactor operated in the differential regime (*n*-hexane conversion <10 %).

3 Results

3.1 Specific Surface Area (SBET)

The results of the specific surface area are presented in Table 1. The deposition of the active phases leads to a decrease in the initial SBET of the support. The pore volume and the pore mean diameter also decrease. The values are not dependant on the different contents of manganese and cerium.

3.2 X-ray Diffraction (XRD)

Figures 1 and 2 show the XRD patterns of $Mn_{1-y}Ce_y/Al_2O_3$ and $(MnCu)_{1-y}Ce_y/Al_2O_3$ catalysts. The diffraction lines of the support were identified as transition phases of θ-Al_2O_3 (JCPDS file 35-121) and δ-Al_2O_3 (JCPDS file 4-877). The XRD patterns of all catalysts conserved the diffraction lines of the support and exhibited additional lines corresponding to the phases Mn_2O_3 (JCPDS 6-0540

Table 1 Specific surface area (SBET), and catalytic activity in *n*-hexane combustion

Catalyst	S_{BET}	dp (A)	Vp (cm^3/g)	Catalytic activity	
				T_{50} (°C)	T_{90} (°C)
Al_2O_3	100.8	52.4	0.13		
MnO_x/Al_2O_3	77.4	52.7	0.10	266	312
$MnCu/Al_2O_3$	75.7	50.1	0.10	274	302
$(MnCu)_{0.9}Ce_{0.1}/Al_2O_3$	73.3	51.6	0.10	262	298
$(MnCu)_{0.8}Ce_{0.2}/Al_2O_3$	70.7	52.8	0.10	262	298
$(MnCu)_{0.7}Ce_{0.3}/Al_2O_3$	83.7	48.2	0.11	245	284
$Mn_{0.9}Ce_{0.1}/Al_2O_3$	81.4	52.8	0.12	268	310
$Mn_{0.8}Ce_{0.2}/Al_2O_3$	94.1	50.8	0.13	254	290
$Mn_{0.7}Ce_{0.3}/Al_2O_3$	80.1	48.1	0.10	240	272

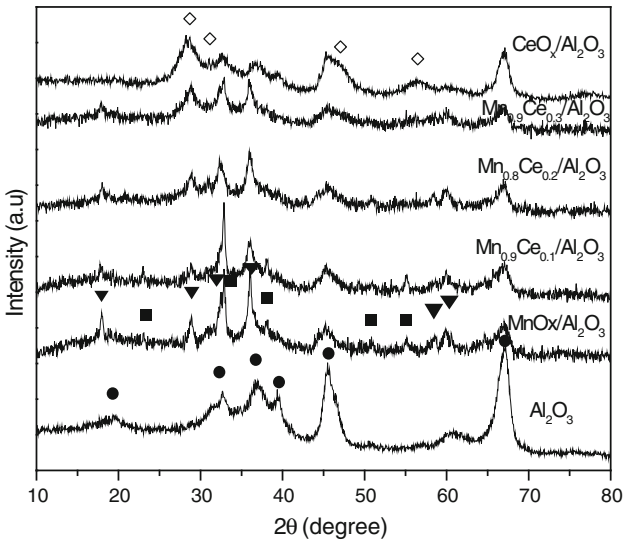

Fig. 1 X-ray diffractograms of Al_2O_3 support and the $Mn_{1-y}Cey/Al_2O_3$ catalysts. *Black circle* θ−δ Al_2O_3 JCPDS files (35-121, 4-877); *black square* Mn_2O_3 JCPDS files (6-0540, 01-089-2809); *black triangle* Mn_3O_4 JCPDS file (01-089-4837); *white rhombus* CeO_2 JCPDS file (43-1002)

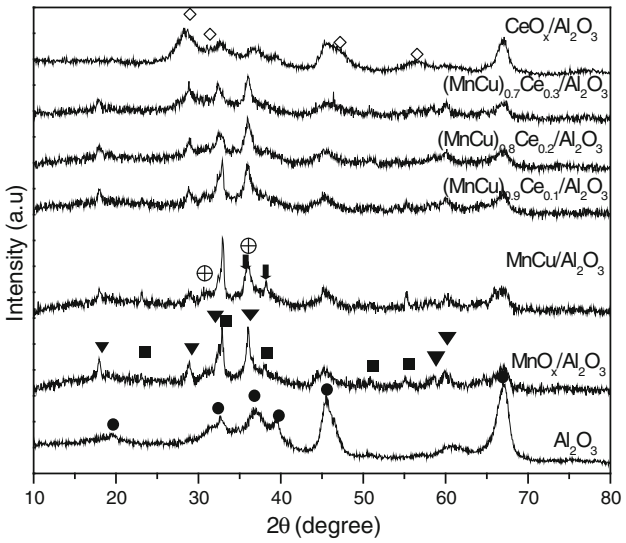

Fig. 2 X-ray diffractograms of Al_2O_3 support and the $(MnCu)_{1-y}Cey/Al_2O_3$ catalysts. *Black circle* θ-δ Al_2O_3 JCPDS files (35-121, 4-877); *black square* Mn_2O_3 JCPDS files (6-0540, 01-089-2809); *black triangle* Mn_3O_4 JCPDS file (01-089-4837); *white rhombus* CeO_2 JCPDS file (43-1002); *Encircled multi* Mn_2CuO_4 spinel JCPDS file (11-0480); *down point arrow* CuO JCPDS file (01-089-253)

and 01-089-2809) and Mn_3O_4 (JCPDS 01-089-4837). The $MnCu/Al_2O_3$ catalysts also exhibited the diffraction lines corresponding to $CuMn_2O_4$ spinel phase (JCPDS 11-0480) and CuO (JCPDS 01-089-2531). The addition of Ce was evidenced by the presence of CeO_2 phase (JCPDS 43-1002), but this phase was only detected by XRD in samples with high content of Ce. The intensity of Mn_2O_3 and Mn_3O_4 phases decreased with the increase in Ce content.

3.3 X-ray Photoelectron Spectroscopy (XPS)

The XPS data are presented in Table 2, and are expressed as atomic ratios of the elements. For all catalysts, Mn2p/Al2p atomic ratios were similar (around 0.2), independently from the presence of Cu or Ce. However, $Mn_{0.8}Ce_{0.2}/Al_2O_3$ and $Mn_{0.7}Ce_{0.3}/Al_2O_3$ catalysts presented exceptional values of 0,33 and 0,16 respectively. The Mn2p spectra of catalysts are shown in Figs. 3 and 4. The Mn 2p3/2 binding energies ranged from 641.9 to 642,6 eV. It is worth noting that the determination of the oxidation states is particularly problematic in the case of manganese oxides due to the overlapping of energy ranges for the various oxidation states of manganese [29, 30]. However the fact that the Mn 2p3/2 peak is rather broad may imply the coexistence of more than one manganese species at the surface of catalysts. The oxidation state of cerium could be deduced from the intensity of the peak at 917 eV, ascribable to CeO_2. The area of this peak may be used for semi-quantitative estimation of the relative amount of cerium present in the samples as Ce^{4+}.

Table 2 XPS results

Catalyst	Mn/Al	Cu/Al+Mn+Ce	%Ce^{4+}	O_l	O_{ad}	Ow
MnO_x/Al_2O_3	0.20			63.6	29.9	6.4
$MnCu/Al_2O_3$	0.18			63.6	32.2	4.2
$(MnCu)_{0.9}Ce_{0.1}/Al_2O_3$	0.20	0.14	7.4	59.6	38.0	2.4
$(MnCu)_{0.8}Ce_{0.2}/Al_2O_3$	0.18	0.13	8.1	60.1	38.2	1.7
$(MnCu)_{0.7}Ce_{0.3}/Al_2O_3$	0.19	0.15	12.1	62.1	37.9	
$Mn_{0.9}Ce_{0.1}/Al_2O_3$	0.19		4.7	57.1	37.7	5.2
$Mn_{0.8}Ce_{0.2}/Al_2O_3$	0.33		9.5	64.9	35.1	
$Mn_{0.7}Ce_{0.3}/Al_2O_3$	0.16		10.5	61.6	38.3	

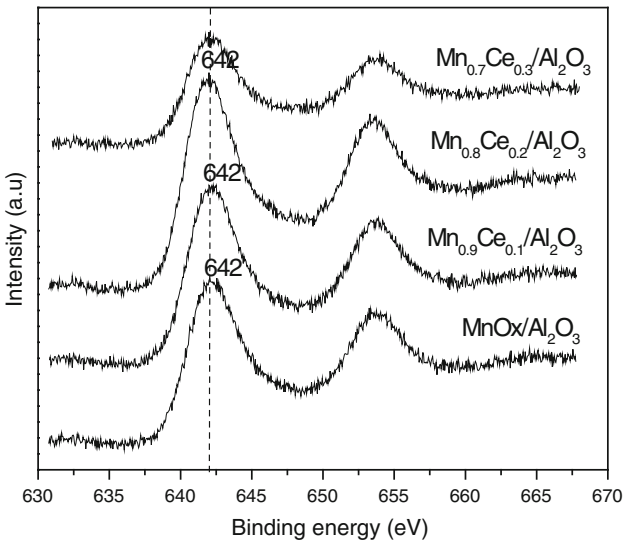

Fig. 3 XPS spectra of the Mn2p region of $Mn_{1-y}Cey/Al_2O_3$ catalysts

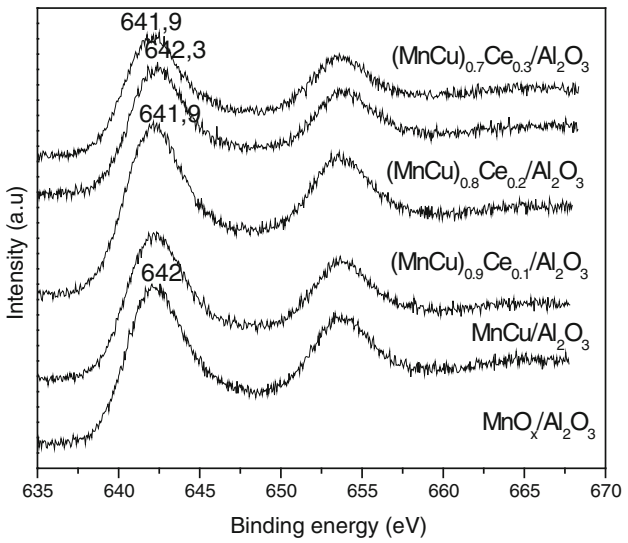

Fig. 4 XPS spectra of the Mn2p region of $(MnCu)_{1-y}Cey/Al_2O_3$ catalysts

This particular peak did not appear in the Ce 3d spectrum of Ce_2O_3 [31] or $CeAlO_3$ [32]. In pure CeO_2 this peak represents 14 % of the total integrated intensity of the Ce3d

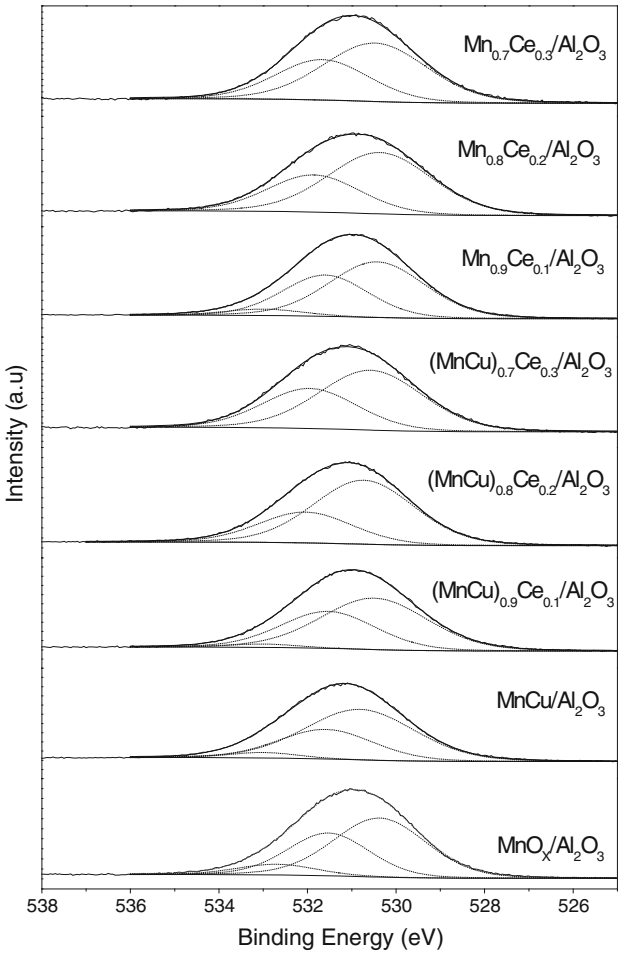

Fig. 5 XPS spectra of O1s region of all catalysts

overall peak [33, 34]. In our catalysts this value is lower than 14 %, indicating the presence of Ce^{3+} in addition to Ce^{4+} in all the samples. The O 1s spectrum of all samples presented a main peak at around 530–531 eV (Fig. 5). By deconvoluting this peak, three components are distinguished, namely the low binding energy peak at 529.8–530.1 eV, ascribed to lattice oxygen, O_l (O_2^{2-}), the medium binding energy peak 531.3 eV, assigned to surface adsorbed oxygen, O_{ad}, (O^{2-} or O^-), OH groups and oxygen vacancies; and finally the high binding energy peak

533.0 eV, likely to be associated with adsorbed molecular water [35]. The relative abundances of O_l and O_{ad} species are listed in Table 2. As expected, the most abundant component in all samples was the lattice oxygen. On the other hand, the highest amount of O_{ad} species was detected in $Mn_{0.7}Ce_{0.3}/Al_2O_3$ catalyst.

3.4 Temperature Programmed Reduction (TPR)

Figure 6 shows the TPR profiles of MnO_x/Al_2O_3 and $Mn_{1-y}Ce_y/Al_2O_3$ catalysts. MnO_x/Al_2O_3 catalyst presents two reduction signals with maxima at around, 314 and 427 °C. The reduction sequence is probably: $Mn^{+4} \rightarrow Mn^{+3} \rightarrow Mn^{+2}$. The T_{onset} reduction temperatures of catalysts containing cerium are lower than that of MnO_x/Al_2O_3 catalyst and decrease with cerium content. A broadening of the first signal is also observed. This could be due to an overlapping of two signals with intensities that become similar when the Ce content is increased. One of the overlapped signals could be attributed to the reduction of surface reactive species with different Mn–O strengths that are not strongly stabilized within the oxide lattice, or to the reduction of manganese species with higher oxidation state, Mn^{4+}. The other signal may be attributed to the reduction of Mn_2O_3 to Mn_3O_4. The second and more intense reduction signal could be associated not only with the reduction of Mn_3O_4 to MnO but with the reduction of CeO_2 as well. As it can be seen in Fig. 6 the reduction of CeO_2/Al_2O_3 starts at 320 °C and presents a broad signal with maxima at 450 and 570 °C. A progressive shift of the second reduction signal to higher temperatures is also observed.

Figure 7 shows the TPR profiles of MnO_x/Al_2O_3, $MnCu/Al_2O_3$ and $(MnCu)_{1-y}Ce_y/Al_2O_3$ catalysts. The addition of Cu to the MnO_x/Al_2O_3 catalyst generates four reduction signals having their maxima at 362 and 427 °C, which could be attributed to the reduction of the manganese oxide and the signal at 276 °C to the reduction of copper. The small peak at temperature region of 200–210 °C could be associated with the reduction of easily reducible surface species of manganese. The $(MnCu)_{1-y}$

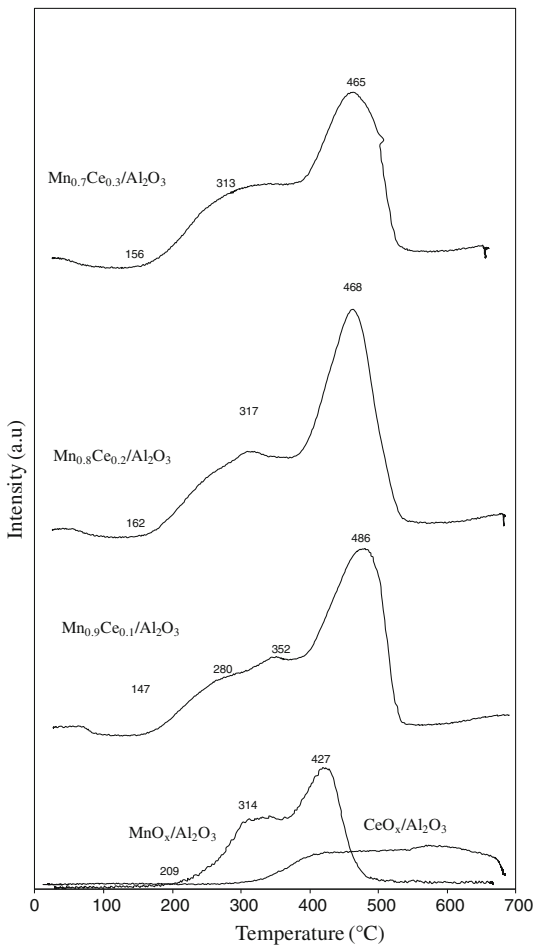

Fig. 6 Temperature programmed reduction profiles of $Mn_{1-y}Cey/Al_2O_3$ catalysts

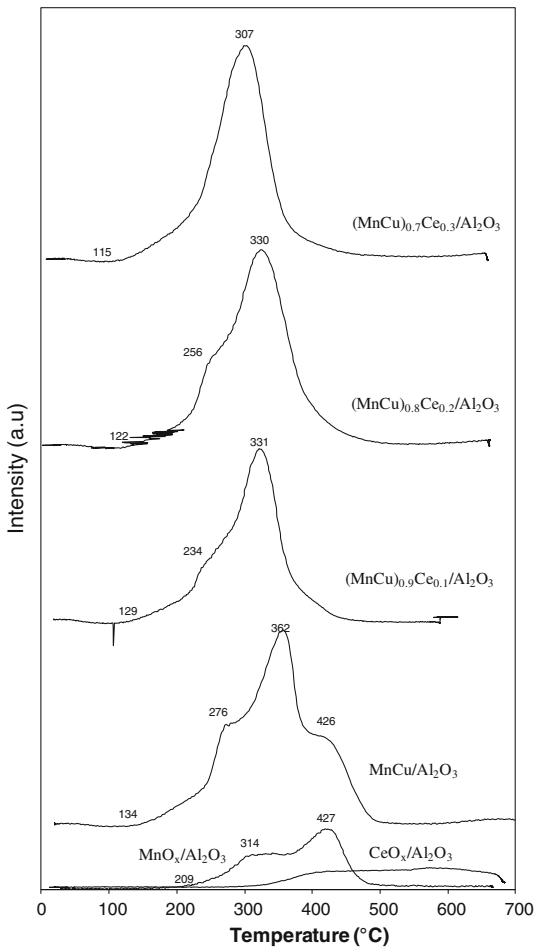

Fig. 7 Temperature programmed reduction profiles of $(MnCu)_{1-y}Cey/Al_2O_3$ catalysts

Ce_y/Al_2O_3 catalysts present only one reduction signal with a small shoulder at low temperatures. A shift of these signals to lower temperatures is observed with the increase in Ce content. The T_{onset} reduction temperatures considerably decrease when the cerium content is increased. Based on above speculations, the TPR curves were deconvoluted using set of two or four peaks related to the reduction of the active component species. The deconvolution of the reduction curves corresponding to MnO_x/Al_2O_3, $MnCu/Al_2O_3$, $(MnCu)_{0.7}Ce_{0.3}/Al_2O_3$ and $Mn_{0.7}Ce_{0.3}/Al_2O_3$ catalysts is shown as an example in Fig. 8. Considering the amount of hydrogen consumed calculated from the integration of the first component (Table 3), it is possible to assume that $Mn_{0.7}Ce_{0.3}/Al_2O_3$ catalysts presents the highest amount of surface manganese oxide or manganese species with a higher oxidation state.

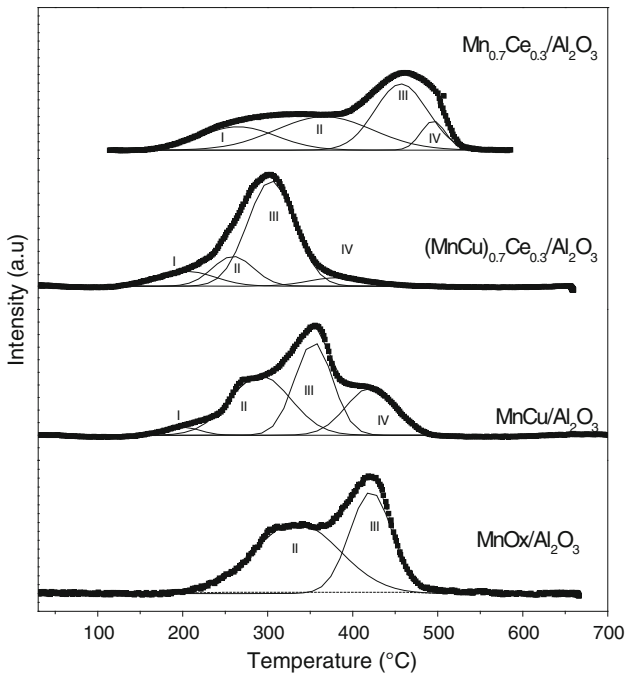

Fig. 8 Deconvolution of the TPR spectra

3.5 Catalytic Activity

The results of catalytic activity in *n*-hexane combustion are presented in Fig. 9 and Table 1. It is clearly observed that the addition of Cu does not modify the catalytic behaviour of MnO_x/Al_2O_3 catalyst. However, the addition of cerium clearly increases the catalytic activity of the system. Higher conversion of *n*-hexane was obtained with a higher cerium content. Comparing T_{50} and T_{90}, (reaction temperatures corresponding to 50 and 90 % of hexane conversion), between MnO_x/Al_2O_3 and $Mn_{0.7}Ce_{0.3}/Al_2O_3$ catalysts, differences of 26 and 40 °C respectively were obtained. The presence of both elements, Cu and Ce, causes an increase of the catalytic activity, evidenced by the lower reaction temperatures obtained. This effect is more important for $(MnCu)_{0.7}Ce_{0.3}/Al_2O_3$, the higher cerium content catalyst. However the activity of this catalyst resulted lower than that of $Mn_{0.7}Ce_{0.3}/Al_2O_3$. The activation energy values obtained under differential conditions were 24 and 33 kJ/mol in average for $Mn_{0.7}Ce_{0.3}/Al_2O_3$ and $(MnCu)_{0.7}Ce_{0.3}/Al_2O_3$ respectively. In all cases CO_2

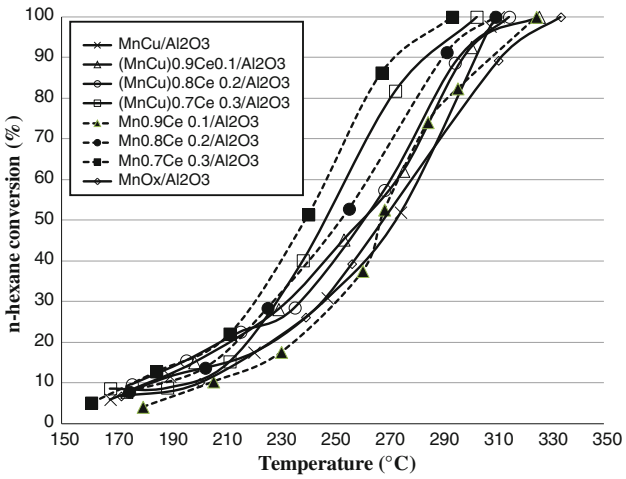

Fig. 9 *n*-hexane conversion as a function of the reaction temperature

Table 3 Hydrogen consumption from TPR results

Catalyst	Hydrogen consumption (mol H_2/gcat)			
	I	II	III	IV
MnO_x/Al_2O_3		2.86E−04	3.68E−04	
$MnCu/Al_2O_3$	5.67E−05	8.01E−04	7.72E−04	5.06E−04
$(MnCu)_{0.9}Ce_{0.1}/Al_2O_3$	2.98E−05	6.31E−04	6.67E−04	1.43E−04
$(MnCu)_{0.8}Ce_{0.2}/Al_2O_3$	5.03E−05	3.41E−04	1.33E−03	2.11E−04
$(MnCu)_{0.7}Ce_{0.3}/Al_2O_3$	1.97E−04	2.92E−04	1.18E−03	1.19E−04
$Mn_{0.9}Ce_{0.1}/Al_2O_3$	1.66E−04	4.02E−04	4.01E−04	1.63E−04
$Mn_{0.8}Ce_{0.2}/Al_2O_3$	8.43E−05	4.50E−04	4.12E−04	3.77E−04
$Mn_{0.7}Ce_{0.3}/Al_2O_3$	2.36E−04	4.29E−04	4.58E−04	9.56E−05

and H_2O were the only reaction products detected in *n*-hexane combustion reaction.

4 Discussion

The catalytic combustion of VOCs in industrial emissions requires the use of structured supports (monoliths) with a high attrition resistance and a low pressure drop, due to the high flows of the emitted pollutants [36]. Monolithic catalysts are composed by the structural material or substrate and the catalyst itself, which covers the monolith walls, and is usual constituted by an active phase dispersed on a catalytic support. Thus, in this paper we intended to study the characteristics of the active phases deposited on an alumina support. Alumina is widely used as a binder in order to increase the adherence of the active phase with the monolith, and it is also used to increase the exposed surface area. For this purpose, a θ-δ-Al_2O_3 (JCPDS 35-121 and 4-877) with 100 m^2/g^{-1} of specific surface area was used as support, since it has demonstrated very good results as support of manganese oxide catalyst used for the combustion of VOCs [37].

The excellent catalytic activity of manganese oxides in the combustion of several VOCs has been attributed to the numerous oxidation states of manganese and to the high oxygen mobility that its oxides present [38, 39]. It has been reported that the catalytic activity of manganese oxides catalysts could be improved with the addition of transition elements (Fe, Cu, Ni, etc.) or elements that could also present high oxygen mobility as in the case of cerium [40]. Figure 9 and Table 1 clearly show that the addition of Cu did not modify the catalytic activity of MnO_x/Al_2O_3 catalyst in contrast to what was expected. Clearly, the reasons of its lower catalytic activity could be the lower specific surface area and lower manganese dispersion on the support evidenced by lower Mn/Al atomic ratio from XPS and the presence of Mn_2CuO_4 phase detected by XRD. Although $CuMn_2O_4$ hopcalite has proved to be an excellent catalyst in total oxidation of CO [41–44], as well as in total combustion of VOCs [43], Mc Cabe and Mitchell [45] showed that the hopcalite was deactivated. On the other hand, Hutchings et al. [46] reported that phases of manganese copper mixed oxides in presence of CuO phase were less active than mixed oxide phases in presence of Mn_2O_3 in CO oxidation. In a previous paper a MnCu catalyst with 9:1 molar ratio synthesized by a co-precipitation method was found to be very active in combustion reactions due to the presence of highly dispersed manganese oxides species, and to the presence of an incomplete spinel, $Mn_{1.5}Cu_{1.5}O_4$. In this work traces of CuO and Mn_2CuO_4 phase were detected by XRD (Fig. 1). Evidently the synthesis method plays an important role. The co-precipitation method provides a high inter-dispersion of copper and manganese and thus, the synthesis conditions could produce multiple arrangements such as solid solutions. With impregnation to incipient wetness, the method used in this work, it is not possible to reproduce the catalyst previously published [27]. Tanaka et al. [47] reported that CuMn precipitate calcination over 500 °C resulted in the CuMn-spinel oxide in different phase according to the different calcination temperature. $CuMn_2O_4$ spinel single phase was formed at 500 °C, whereas the formation of $Cu_{1.5}Mn_{1.5}O_4$ and Mn_2O_3 was formed at 700 °C. Phases obtained with the calcination temperature used in this work are in agreement with these results.

On the other hand, the addition of cerium improved the catalytic activity of the system. Cerium oxides in presence of transition metal oxides have shown to promote oxygen storage and release, to enhance oxygen mobility, to form surface and bulk vacancies, and to improve the catalyst redox properties of the composite oxide [48]. When both elements—Cu and Ce—are present, the increase in catalytic activity is more noticeable with the increase in cerium content. Thus, a high content of cerium generates more active species on the catalyst surface which promote the oxidation of *n*-hexane at lower temperatures. From XRD results (Fig. 2) it can be deduced that the increase in Ce content induce the formation of MnO_x phases with low crystallinity. Structural defects associated with the poor crystallinity can lead to the presence of oxygen vacancies in the synthesized materials [27]. The oxygen vacancies are recognized as adsorption–desorption centers for oxygen from the gaseous phases and consequently they would act as active sites in oxidation reactions. Higher oxygen mobility could be also deduced from TPR results (Fig. 7). $(MnCu)_{1-y}Ce_y/Al_2O_3$ catalysts present only one reduction signal with a small shoulder at low temperatures which shifts to lower temperatures with the increase in Ce content. It has been reported that in CuCe catalysts, cerium favors the CuO species dispersion being easily reduced due to the Cu spill over [49]. Thus, the presence of a single reduction signal in $(MnCu)_{1-y}Ce_y/Al_2O_3$ catalysts could be attributed to the presence of these Cu species and also to the strong interaction of manganese and cerium. This strong interaction would favor a higher oxygen mobility [50, 51]. Li et al. [52] also found that the reduction of $Ce_{1-x}Mn_xO_2$ was markedly promoted by impregnating it with CuO, and the reduction of CuO was improved by $Ce_{1-x}Mn_xO_2$. A redox interaction occurred between CuO and $Ce_{1-x}Mn_xO_2$ which facilitated the activation of surface oxygen for the oxidation of benzene. A slightly higher amount of surface Cu species were detected by XPS (Table 2) on $(MnCu)_{0.7}Ce_{0.3}/Al_2O_3$. However, the

difference among these values is not significant in order to explain the higher catalytic activity of this catalyst. The relative surface concentration of O_{ad} that has higher mobility than lattice oxygen may actively take part in the oxidation process and greatly contribute to the catalyst activity. Table 2 shows that the addition of Ce also increases the relative abundance of O_{ad} determined by XPS analysis. In general, mixed oxides samples contain a higher amount of O_{ad} species than pure oxides. Though, the O_{ad} values resulted similar and around 38 % for the three $(MnCu)_{1-y}Ce_y/Al_2O_3$ catalysts. The highest difference was found in the proportion of Ce^{4+}. The existence of Ce^{3+} was detected in all the samples, and this was favourable since it is also an evidence of oxygen vacancies on the surface. However, higher the content of Ce higher the proportion of Ce^{4+}, which clearly plays an important role in the catalyst performance.

The addition of Ce also increased the catalytic performance of MnO_x/Al_2O_3 catalysts in absence of Cu. Catalysts with higher Ce content presented lower reaction temperatures. In fact, $Mn_{0.7}Ce_{0.3}/Al_2O_3$ resulted the most active catalyst of all prepared, reaching 50 % of *n*-hexane conversion at 240 °C. The low crystallinity of manganese phases was also detected in this catalyst with high content of Ce, thus, the presence of oxygen vacancies are expected. Although, the most abundant component in all samples was the lattice oxygen, the highest amount of O_{ad} species was detected in $Mn_{0.7}Ce_{0.3}/Al_2O_3$ catalyst. It becomes difficult to establish a direct relationship between the reducibility and the catalytic activity since $Mn_{0.7}Ce_{0.3}/Al_2O_3$ catalyst presented higher reduction temperatures. However, this catalyst presented higher activity, evidenced by the lower reaction temperatures and lower activation energy values in comparison with $(MnCu)_{0.7}Ce_{0.3}/Al_2O_3$. The higher reduction temperatures of the second signal could be attributed to the presence of cerium ions in lower oxidative state, which are in strong interaction with manganese and the alumina support. Although CeO_2 was the only phase detected by XRD, the presence of Ce^{3+} at the surface of catalyst was observed by XPS technique, indicating also the presence of oxygen vacancies in the CeO_2 formed on the surface. The first reduction signal was attributed to the reduction of surface reactive species or to the reduction of manganese species with higher oxidation state, Mn^{4+}, overlapped to the reduction signal of Mn_2O_3 to Mn_3O_4. If the amount of hydrogen consumed calculated from the integration of the first component (Table 3) is considered, it is possible to assume that $Mn_{0.7}Ce_{0.3}/Al_2O_3$ catalysts presents the highest amount of surface manganese oxide or manganese species with a higher oxidation state. It is well known that higher oxidation state of manganese species is preferable for oxidation reactions over the manganese containing catalysts [53, 54].

5 Conclusions

Supported MnCuCe and MnCe catalysts presented an excellent catalytic activity in total combustion of *n*-hexane in which the main reaction products were CO_2 and H_2O. The addition of Cu did not enhance the catalytic activity of MnO_x/Al_2O_3 due to the formation of the complete Mn_2CuO_4 spinel. The presence of cerium favored the formation of manganese oxide species with low crystallinity, with high oxygen mobility and high oxygen vacancies. A higher content of Ce was necessary to obtain catalysts with higher oxidation state of Mn and Ce species, explaining thus, the higher catalytic activity of $(MnCu)_{0.7}Ce_{0.3}/Al_2O_3$ and $Mn_{0.7}Ce_{0.3}/Al_2O_3$ catalysts.

Acknowledgments The financial support from UNSL, CONICET and ANPCyT of Argentina is gratefully acknowledged.

References

1. Larsson PO, Andersson A (1998) J Catal 179:72
2. Papaefthimiou P, Ioannides T, Verykios XE (1998) Appl Therm Eng 18:1005
3. Atkinson R, Arey J (2003) Chem Rev 103:4605
4. Everaert K, Baeyens J (2004) J Hazard Mater B 109:113
5. Spivey J (1987) Ind Eng Chem Res 26:2165
6. Burgos N, Paulis M, Antxustegi MM, Montes M (2002) Appl Catal B 38:251
7. Gil A, Vicente MA, Lambert JF, Gandía LM (2001) Catal Today 68:41
8. van den Brink RW, Louw R, Mulder P (1998) Appl Catal B 16:219
9. Scire S, Minico S, Crisafulli C (2003) Appl Catal B 45:117
10. Larsson PO, Andersson A (2000) Appl Catal B 24:175
11. Martínez-Arias A, Fernández-García M, Soria J, Conesa JC (1999) J Catal 182:367
12. Qi G, Yang RT (2003) J Catal 217:434
13. Liu W, Stephanopoulos MF (1995) J Catal 153:317
14. Avgouropoulos G, Ioannides T, Papadopoulou Ch, Batista J, Hocevar S, Matralis HK (2002) Catal. Today 75:157
15. Avgouropoulos G, Ioannides T (2006) Appl Catal B 67:1
16. Trovarelli A, de Leitenmburg C, Dolcetti G (1997) ChemTech 27:32
17. Yao MH, Baird RJ, Kunz FW, Hoost TE (1997) J Catal 166:67
18. Schmitz PJ, Usmen RK, Peters CR, Graham GW, McCabe RW (1993) Appl Surf Sci 72:181
19. Zafiris GS, Gorte RJ (1993) J Catal 143:86
20. Hori CE, Permana H, Ng KYS, Brenner A, More K, Rahmoeller KM, Belton DN (1998) Appl Catal B 16:105
21. Lin R, Zhong YJ, Luo MF, Liu WP (2001) Indian J Chem A 40:36
22. Arena F, Trunfio G, Negro J, Fazio B, Spadaro L (2007) Chem Mater 19:2269
23. Stobbe ER, de Boer BA, Geus JW (1999) Catal Today 47:161
24. Kim SC, Shim WG (2010) Appl Catal B 98:180
25. Tang X, Li Y, Huang X, Xu Y, Zhu H, Wang J, Shen W (2006) Appl Catal B 62:265
26. Li TY, Chiang SJ, Liaw BJ, Chen YZ (2011) Appl Catal B 103:143
27. Morales MR, Barbero BP, Cadús LE (2008) Fuel 87:1177

28. Avila P, Montes M, Miro E (2005) Chem Eng J 11:11
29. Huang SJ, Walters AB, Vannice MA (2000) J Catal 192:29
30. Park PW, Kil JK, Kung HH, Kung MC (1998) Catal Today 42:51
31. Barr TL, Fries CG, Cariati F, Bart JCJ, Giordano N, Trans Dalton (1983) J Chem Soc 9:1825
32. Shyu JZ, Otto K, Watkins WLH, Graham GW, Belitz RK, Gandhi HS (1988) J Catal 114:23
33. Schmitz P, Usmen R, Peters C, Graam J, McCabe R (1993) Appl Surf Sci 72:181
34. Fernandez-Garcia M, Gomez-Rebollo E, Guerrero Ruiz A, Conesa JC, Soria J (1997) J Catal 172:146
35. Jiratova K, Mikulova J, Klempa J, Grygar T, Bastl Z, Kovanda F (2009) Appl Catal A 361:106
36. Burgos N, Paulis M, Montes M (2003) J Mater Chem 13:1458
37. Aguero FN, Scian A, Barbero BP, Cadús LE (2008) Catal Today 133(135):493
38. Lahousse C, Bernier A, Grange P, Delmon B, Papaefthimiou P, Ionnides T, Verykios X (1998) J Catal 178:214
39. Lamaita L, Peluso MA, Sambeth JE, Thomas HJ (2005) Appl Catal B 611:28
40. Picasso G, Gutierrez M, Pina MP, Erguido J (2007) Chem Eng J 126:119
41. Tichenor BA, Palazzolo MA (1987) Environ Prog 6:172
42. Hutchings GJ, Mirzaei AA, Joyner RW, Siddiqui MRH, Taylor SH (1998) Appl Catal A 166:143
43. Mirzaei AA, Shaterian HR, Habibi M, Hutchings GJ, Taylor SH (2003) Appl Catal A 253:499
44. White WB, Keramidas VG (1972) Spectrochim Acta A 28:501
45. McCabe RW, Mitchell PJ (1984) Ind Eng Chem Prod Res Dev 23:196
46. Hutchings GJ, Mirzaei AA, Joyner RW, Siddiqui MRH, Taylor SH (1998) Appl Catal A 166:143
47. Tanaka Y, Utaka T, Kikuchi R, Takeguchi T, Sasaki K, Eguchi K (2003) J Catal 215:271
48. Larachia F, Pierrea J, Adnota A, Bernis A (2002) Appl Surf Sci 195:236
49. Águila G, Gracia F, Araya P (2008) Appl Catal A 343:16
50. Hu C, Zhu Q, Jiang Z, Chen L, Wu R (2009) Chem Eng J 152:583
51. Blanco G, Cauqui MA, Delgado JJ, Galtayries A, Perez-Omil JA, Rodríguez-Izquierdo JM (2004) Surf. Interface Anal 367:52
52. Li T, Chiang S, Liaw B, Chen Y (2011) Appl Catal B 103:143
53. Kapteijn F, Singoredjo L, Andreini A (1994) Appl Catal B 3:173
54. Park JS, Doh DS, Lee KY (2000) Top Catal 10:127